# Core Chlorination Position Governs Charge Transport and Efficiency in Small-Molecule Acceptors for Organic Solar Cells

Jinjin Wang,†[a] Han Tian,†[a] Jiaxu Che,[b] Chuanlin Gao,[b] Zeyuan Ye,[a] Yufei Wang,[b] Guangye Zhang, [b] Zhenghui Luo,*[a] Chuluo Yang[a]

[a]Guangdong Provincial Key Laboratory of New Energy Materials Service Safety, Shenzhen Key Laboratory of New Information Display and Storage Materials, College of Materials Science and Engineering, Shenzhen University, Shenzhen 518060, China. Email: zhhuiluo@szu.edu.cn.

[b]College of New Materials and New Energies Shenzhen Technology University, Shenzhen 518118, China.

‡ These authors contributed equally to this work.

## 1. Synthesis and Characterizations

**General information:** All solvents and reagents were used as received from commercial sources and used without further purification unless otherwise specified. All reactions were heated by metal sand bath. $^{1}$H NMR (400 MHz) and $^{13}$C NMR (100 MHz) spectra were measured on a MERCURYVX300 spectrometers. Mass spectra were recorded on a Shimadzu spectrometer. High-resolution mass spectrometry was carried out on Thermo Scientific TM Q-Exactive.

**Cyclic Voltammetry (CV):** CV measurements were performed on a CHI660A electrochemical workstation in a solution of tetrabutylammonium hexafluorophosphate ($Bu_4NPF_6$, 0.1 M) in acetonitrile at a scan rate of 50 mV $s^{-1}$, glassy carbon electrode, platinum wire and an Ag/AgCl electrode were used as working electrode, counter electrode, and reference electrode, respectively.

**Atomic force microscopy (AFM)**. AFM measurements were performed by using a Dimension ICON under atmosphere conditions at room temperature. All film samples were spin-cast on glass/ITO substrates.

**Grazing incidence wide-angle X-ray scattering (GIWAXS):** GIWAXS experiments were carried out on an XEUSS 3.0 UHR SAXS/WAXS system (XENOCS, France). A Eiger2 R 1M 2-dimensional detector with 0.075 mm×0.075 mm active pixels were utilized in integration mode. The sample-to-detector distance is settled at 100 mm for GIWAXS measurement. The samples for GIWAXS test were prepared by casting solution onto silicon wafer substrates (ca. 10 mm × 10 mm), and the active layers were prepared using exactly the same concentration and same procedures as those for *J–V* measurements. The coherence length was calculated using the Scherrer equation: CCL = 2πK/FWHM, where *K* is a dimensionless shape factor, normally with a value of 0.9. FWHM is the full with at half maximum of peak and $\theta$ is Bragg's angle (scattering angle).

## 2. Device fabrication and characterization

**Device fabrication.** The OSCs with the structure of ITO/PEDOT:PSS/Active Layer/PNDIT-F3N/Ag were fabricated. The indium tin oxide (ITO) glass substrates were cleaned three times with ethanol using ultrasonic wabes, for 15 min each time.

Then, the ITO substrate was treated with UV ozone for 15 min. the PEDOT:PSS (Heraues Clevios P VP AI 4083) solution was spin-coaed on the UV ozone-treated ITO substrate at 5000 rpm for 25 s, and then dried at 150 $^{o}$C for 15 min in air. For D18: *p*-Cl-DOP and D18:*m*-Cl-DOP solution, the total concentration was 10 mg/mL (weight ratio, w/w, 1:1), dissolved in chloroform at 75 $^{o}$C. these active layers were spin-coaed at 2700 rpm onto substrates for 25 s, then treated by 100 $^{o}$C thermal annealing for 5 min. For above devices, a methanol with 1% vol acetic acid blend solution of PNDIT-F3N at a concentration of 1 mg/mL was spin-coated onto the active layer at 3000 rpm for 25 s. Finally, around 100 nm of Ag was evaporated under $1\times10^{-4}$ Pa through a shadow mask (area of the OPV devices 0.04012 cm$^{-2}$).

**Device characterization.** The current density-voltage (*J-V*) curves of all encapsulated devices were measured using a Keithley 2400 Source Meter under AM 1.5G (100 mW cm$^{-2}$) using an Enlitech solar simulator. The light intensity was calibrated using a standard Si diode with KG5 filter to bring spectral mismatch to unity. EQEs were measured using an Enlitech QE-S EQE system equipped with a standard Si diode. Monochromatic light was generated from a Enlitech 300 W lamp source. Capacitance-frequency Impedance spectroscopy, Photo-CELIV measurements were performed using commercially available Paios system (FLUXiM AG).

**Transient photovoltage (TPV) and transient photocurrent (TPC) measurements:** In TPV measurements, the devices were placed under background light bias enabled by a focused Quartz Tungsten-Halogen Lamp with an intensity of similar to working devices, *i.e.,* the device voltage matches the open-circuit voltage under solar illumination conditions. A digital oscilloscope was used to acquire the TPV signal at the open-circuit condition. TPC signals were measured under short-circuit conditions under the same excitation wavelength without background light bias.

**FTPS-EQE and EL-EQE measurements.** FTPS-EQE was measured using an integrated system (PECT-600, Enlitech), where the photocurrent was amplified and modulated by a lock-in instrument. EL-EQE measurements were performed by applying external voltage/current sources through the devices (REPS-Pro, Enlitech). All of the devices were prepared for EL-EQE measurements according to the optimal

device fabrication conditions. EL-EQE measurements were carried out from 0 to 1.8 V.

**Space-charge-limited-current (SCLC):** The carrier transport capabilities of the photoactive layer were investigated using the space-charge-limited-current (SCLC) method. The architecture of ITO/PEDOT: PSS/D18: Acceptors/$MoO_3$/Ag was used as the hole-only device to measure the hole mobility, and the electron mobility was measured by the electron-only device of ITO/ZnO/D18: Acceptors/PNDIT-F3N/Ag configuration. The processing conditions used for the active layers were the optimized conditions. In the dark condition, the charge mobility was extracted and recorded by fitting the current density-voltage curves with the Mott-Gurney equation. Though fitting the dark current to single carrier SCLC to determine the mobility, and it is were calculated from the equation:

$$J = \frac{9}{8}\varepsilon_0\varepsilon_r\mu_h\frac{V^2}{d^3}$$

where $J$, $\varepsilon_0$, $\varepsilon_r$, $\mu_h$, $d$, and $V$ are referred to the current, the permittivity of free space, the relative permittivity of the material, the zero-field mobility, the thickness of the active layer, and the effective voltage, respectively. The effective voltage is obtained from the equation $V = V_{appl}$-$V_b$-$V_s$, where $V_{appl}$, $V_b$, and $V_s$ are the applied voltage, the offset voltage and the voltage drop, respectively.

**The analysis of $J_{ph}$ vs $V_{eff}$ relationships:** The definition of $J_{ph}$ is the current density under illumination ($J_L$) minus the dark current density ($J_D$), and $V_0$ refers to the voltage value when $J_{ph} = 0$. Accordingly, $V_{eff} = V_0 - V_{appl}$, where $V_{appl}$ represents applied voltage, has a clear meaning. Importantly, when $V_{eff}$ reaches a high value (> 2V) it is normally believed that generated excitons are fully collected, in which $J_{ph}$ is equal to saturated current density ($J_{sat}$). Then, we can calculate $J_{SC}/J_{sat}$ and $J_{max}/J_{sat}$ to describe exciton dissociation ($\eta_{diss}$) and charge collection ($\eta_{coll}$) efficiency. $J_{max}$ is the $J_{ph}$ at the maximal output point.

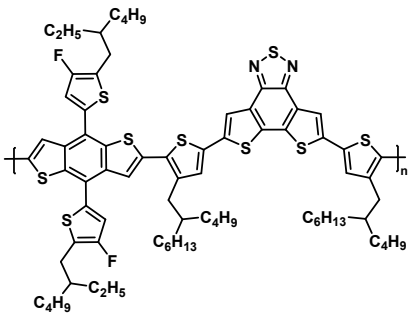

**Scheme S1.** The molecular structure of **D18**

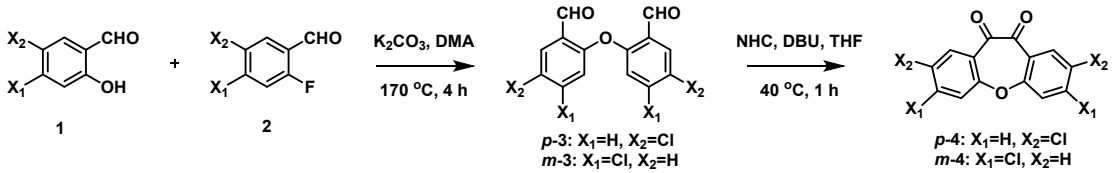


**Scheme S2**. The synthetic route of Compound ***p*-4** and ***m*-4**

***p*-4** and ***m*-4**: The molecules were synthesized by the method of previous literature[1], and $^1$H NMR data were as follows:

***p*-3**: $^1$H NMR (500 MHz, $CDCl_3$) δ 10.38 (s, 2H), 7.94 (dd, *J* = 8.4, 4.2 Hz, 2H), 7.32 (dd, *J* = 8.4, 1.2 Hz, 2H), 6.95 (d, *J* = 1.8 Hz, 2H). HRMS (m/z) $[M+H]^+$ calcd. For ($C_{15}H_8Cl_2O_3$): 294.9928. Found: 294.9921. ***m*-3**: $^1$H NMR (400 MHz, $CDCl_3$) δ 10.39 (s, 2H), 7.93 (d, *J* = 2.7 Hz, 2H), 7.53 (dd, *J* = 8.8, 2.7 Hz, 2H), 6.91 (d, *J* = 8.8 Hz, 2H). HRMS (m/z) $[M+H]^+$ calcd. For ($C_{15}H_8Cl_2O_3$): 294.9928. Found: 294.9923.

***p*-4**: $^1$H NMR (500 MHz, $CDCl_3$) δ 7.96 (d, *J* = 8.5 Hz, 2H), 7.46 (d, *J* = 1.9 Hz, 2H), 7.35 (dd, *J* = 8.5, 1.9 Hz, 2H). HRMS (m/z) $[M+H]^+$ calcd. For ($C_{15}H_6Cl_2O_3$): 292.9772. Found: 292.9762. ***m*-4**: $^1$H NMR (500 MHz, $CDCl_3$) δ 7.99 – 7.95 (m, 2H), 7.65 – 7.60 (m, 2H), 7.41 (d, *J* = 8.7 Hz, 2H). HRMS (m/z) $[M+H]^+$ calcd. For ($C_{15}H_6Cl_2O_3$): 292.9772. Found: 292.9760.

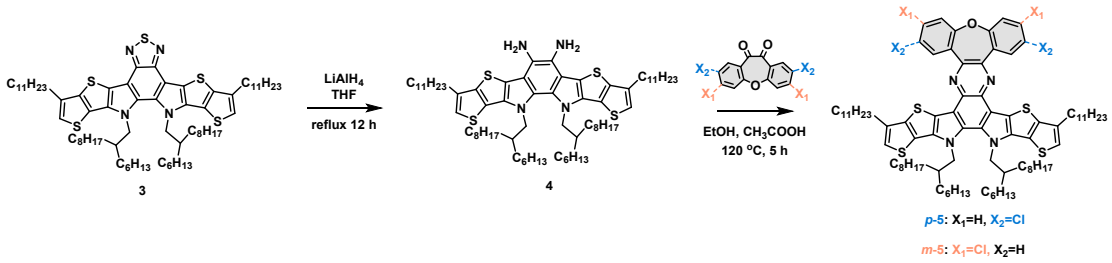


**Scheme S3**. The synthetic route of Compound ***p*-5** and ***m*-5**

Synthesis of compound ***p*-5** and ***m*-5**: Under the protection of nitrogen, compound **3** (1.0 eq.) was dissolved in anhydrous THF, then, a solution of $LiAlH_4$ (1M, 8.0 eq.) was slowly added to the mixed solution. The resulting mixture was stirred and heated to 70 ℃ overnight, after that, the mixture was gently added to the ice cube and extracted with dichloromethane. The organic phase was dried over anhydrous $Na_2SO_4$. The crude product was dissolved in anhydrous ethanol(10 mL) and acetic acid（10 mL）, then 2,3-dihydro-1H-isoquinoline-1,4-dione(2.0 eq.) were added to the solution in turn. The mixture was stirred at 120 ℃ for 5 hours, and then the mixture was extracted with dichloromethane. Finally, the crude product was purified by column chromatography using PE/EA (10:1, v/v) as eluent over silica gel to afford viscous dark green solid with 70% and 71% yield, respectively.

$^1$H NMR data were as follows:

***p*-5:** $^1$H NMR (500 MHz, $CDCl_3$) δ 8.49 (d, *J* = 2.6 Hz, 2H), 7.48 (dd, *J* = 8.6, 2.6 Hz, 2H), 7.35 (d, *J* = 8.6 Hz, 2H), 7.05 (s, 2H), 4.70 (d, *J* = 7.8 Hz, 4H), 2.89 (t, *J* = 7.6 Hz, 4H), 2.26 – 2.12 (m, 2H), 1.95 – 1.84 (m, 4H), 1.43 – 1.20 (m, 42H), 1.01 – 0.88 (m, 32H), 0.80 (d, *J* = 7.3 Hz,8H), 0.70 (t, *J* = 7.2 Hz, 6H). $^{13}$C NMR (125 MHz, CDCl3) δ 158.42, 144.39, 143.52, 137.74, 137.03, 135.00, 133.20, 131.56, 131.40, 131.28, 130.62, 123.58, 122.51, 122.29, 119.14, 117.51, 55.10, 38.70, 31.98, 31.86, 31.67, 30.53, 30.48, 29.76, 29.70, 29.67, 29.59, 29.55, 29.47, 29.42, 29.21, 28.94, 25.56, 22.75, 22.65, 22.54, 14.17, 14.12, 14.03. $[M+H]^+$ calcd. For ($C_{87}H_{120}Cl_2N_4OS_4$): 1422.7722. Found: 1423.7770.

***m*-5:** $^1$H NMR (500 MHz, $CDCl_3$) δ 8.45 (d, *J* = 8.4 Hz, 2H), 7.51 (dd, *J* = 8.4, 2.0 Hz, 2H), 7.43 (d, *J* = 2.0 Hz, 2H), 7.03 (s, 2H), 4.67 (d, *J* = 7.7 Hz, 4H), 2.86 (t, *J* = 7.7 Hz, 4H), 2.20 – 2.10 (m, 2H), 1.89 (dd, *J* = 14.9, 7.5 Hz, 4H), 1.42 – 1.12 (m,

36H), 1.01 – 0.84 (m, 36H), 0.78 (t, $J$ = 7.3 Hz, 11H), 0.67 (t, $J$ = 7.2 Hz, 6H). $^{13}$C NMR (126 MHz, $CDCl_3$) δ 159.94, 144.72, 143.41, 137.73, 136.93, 136.36, 134.90, 132.49, 131.45, 130.44, 126.56, 123.63, 122.37, 121.45, 119.13, 117.58, 55.09, 38.71, 31.99, 31.86, 31.67, 30.53, 30.47, 29.77, 29.72, 29.70, 29.62, 29.56, 29.55, 29.48, 29.43, 29.21, 28.93, 25.56, 22.76, 22.65, 22.54, 14.18, 14.12, 14.03. $[M+H]^+$ calcd. For ($C_{87}H_{120}Cl_2N_4OS_4$): 1422.7722. Found: 1423.7810.

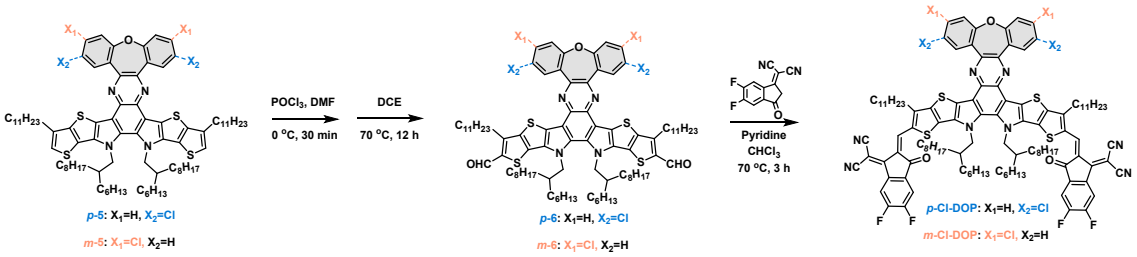


**Scheme S4**. The synthetic route of Compound ***p*-Cl-DOP** and ***m*-Cl-DOP**

Synthesis of compound ***p*-6** and ***m*-6:** $POCl_3$ (3 mL) was added dropwise to a solution of anhydrous *N*, *N*-dimethylformamide (DMF) (8 mL) at 0°C under $N_2$ atmosphere and stirred at room temperature for 30 min. ***p*-5** or ***m*-5** dissolved in 20 mL anhydrous 1,2-dichloroethane (DCE) was add to the above solution and stirred at 70 °C for 12 h under $N_2$ atmosphere. Then, the reaction mixture is quenched by stirring with water and extracted with dichloromethane. Finally, the crude product was purified by column chromatography using PE:DCM (2:1, v/v) as eluent over silica gel to afford red solid with 80% and 84% yield, respectively.

$^1$H NMR data were as follows:

***p*-6:** $^1$H NMR (400 MHz, $CDCl_3$) δ 10.17 (d, $J$ = 2.0 Hz, 2H), 8.44 (d, $J$ = 2.3 Hz, 2H), 7.52 – 7.45 (m, 2H), 7.36 (dd, $J$ = 8.5, 2.0 Hz, 2H), 4.71 (d, $J$ = 6.5 Hz, 4H), 3.24 (d, $J$ = 6.8 Hz, 4H), 2.14 (s, 2H), 1.97 (s, 4H), 1.57 (s, 9H), 1.20 (td, $J$ = 14.1, 4.8 Hz, 37H), 1.01 – 0.82 (m, 36H), 0.84 – 0.76 (m, 10H), 0.69 (t, $J$ = 5.8 Hz, 6H). $^{13}$C NMR (100 MHz, $CDCl_3$) δ 181.85, 158.50, 147.04, 145.47, 144.46, 137.42, 137.02, 135.18, 132.66, 132.63, 131.52, 131.21, 131.09, 129.65, 127.28, 122.48, 118.17, 55.33, 38.92, 31.92, 31.80, 31.59, 31.46, 30.51, 30.42, 30.22, 29.73, 29.67, 29.63, 29.57, 29.43,

29.40, 29.35, 29.19, 28.16, 25.51, 22.70, 22.61, 22.52, 14.13, 14.09, 14.00. $[M+H]^+$ calcd. For ($C_{88}H_{121}Cl_2N_4O_3S_4$): 1478.7620. Found: 1479.7658.

***m*-6:** $^1$H NMR (400 MHz, $CDCl_3$) δ 10.16 (s, 2H), 8.40 (d, *J* = 8.4 Hz, 2H), 7.52 (dd, *J* = 8.4, 2.0 Hz, 2H), 7.45 (d, *J* = 2.0 Hz, 2H), 4.70 (d, *J* = 7.8 Hz, 4H), 3.24 (t, *J* = 7.6 Hz, 4H), 2.13 (s, 2H), 1.99 – 1.90 (m, 4H), 1.39 – 1.17 (m, 36H), 1.00 – 0.83 (m, 37H), 0.78 (q, *J* = 7.1 Hz, 10H), 0.68 (t, *J* = 7.1 Hz, 6H). $^{13}$C NMR (100 MHz, $CDCl_3$) δ 181.79, 160.03, 146.90, 145.80, 144.37, 137.43, 137.03, 136.88, 135.09, 132.55, 132.35, 129.91, 129.70, 127.14, 126.66, 121.60, 118.28, 55.31, 38.93, 31.93, 31.81, 31.60, 30.65, 30.48, 30.43, 29.73, 29.70, 29.64, 29.56, 29.44, 29.36, 29.34, 29.18, 28.13, 25.52, 22.71, 22.61, 22.52, 14.13, 14.09, 14.00. $[M+H]^+$ calcd. For ($C_{88}H_{121}Cl_2N_4O_3S_4$): 1478.7620. Found: 1479.7668.

Synthesis of six ***p*-Cl-DOP** and ***m*-Cl-DOP** Compound ***p*-6** or ***m*-6** (1.0 eq.) and 2-(5,6-Difluoro-3-oxo-2,3-dihydro-1H-inden-1-ylidene)malononitrile (6.0 eq.) were added dissolved in chloroform (30 mL), then 1mL pyridine ws added, the reaction mixture was stirred for 3 h under 70 ℃. The reaction mixture was allowed to cool down to room temperature. The residue was purified by column chromatography using PE/DCM (1:1 v/v) as eluent on silica gel to afford dark blue solid with 92 % and 90% yield, respectively.

$^1$H NMR data were as follows:

***p*-Cl-DOP:** $^1$H NMR (500 MHz, $CDCl_3$) δ 9.16 (s, 2H), 8.55 (d, *J* = 6.5 Hz, 2H), 8.53 (d, *J* = 6.4 Hz, 2H),8.40 (d, *J* = 2.6 Hz, 2H), 7.71 (t, *J* = 7.5 Hz, 2H), 7.53 (d, *J* = 2.6 Hz, 1H), 7.51 (d, 7.37 *J* = 2.6 Hz, 1H ), 7.38 (s, 1H), 7.36 (s, 1H), 4.85 (d, *J* = 7.8 Hz, 4H), 3.28 (t, *J* = 7.9 Hz, 4H), 2.30 - 2.18 (m, 2H), 1.99 - 1.83 (m, 4H), 1.56 - 1.5 (m 9H), 1.44 - 1.37 (m, 4H), 1.36 - 1.19 (m, 30H), 1.15 - 1.10 (m, 6H), 1.09 - 0.94 (m, 30H), 0.85 (t, *J* = 6.9 Hz, 8H), 0.76 (t, *J* = 7.2 Hz, 6H), 0.70 (t, *J* = 7.0 Hz, 6H). $^{13}$C NMR (125 MHz, $CDCl_3$) δ 186.16, 158.45, 158.25, 154.06, 153.23, 146.48, 146.04, 138.40, 136.17, 135.45, 134.71, 133.48, 133.28, 132.15, 131.52, 130.96, 130.56, 124.49, 124.00, 122.71, 119.63, 119.46, 114.97, 68.08, 55.92, 39.41, 34.89, 34.54, 31.95, 31.74, 31.46, 31.28, 30.70, 30.22, 30.02, 29.85, 29.71, 29.69, 29.59, 29.50, 29.47, 29.39, 29.33, 25.79, 22.71, 22.68, 22.63, 14.13, 14.10. HRMS (m/z) $[M]^+$ calcd.

For ($C_{112}H_{124}Cl_2F_4N_8O_3S_4$): 1902.7992. Found: 1902.8012.

***m*-Cl-DOP:**

$^1$H NMR (500 MHz, $CDCl_3$) δ 9.18 (s, 2H), 8.59 (d, *J* = 6.5 Hz, 1H), 8.57 (d, *J* = 6.4 Hz, 1H), 8.36 (d, *J* = 8.4 Hz, 2H), 7.71 (t, *J* = 7.4 Hz, 2H), 7.53 (dd, *J* = 8.4, 1.8 Hz, 2H), 7.46 (d, *J* = 1.8 Hz, 2H), 4.83 (d, *J* = 7.8 Hz, 4H), 3.27 (t, *J* = 7.8 Hz, 4H), 2.32 - 2.11 (m, 2H), 1.94 - 1.84 (m, 4H), 1.53 (s, 3H), 1.35 - 1.19 (m, 30H), 1.14 - 1.08 (m, 6H), 1.06 - 0.95 (m, 30H), 0.85 (t, *J* = 6.8 Hz, 8H), 0.75 (t, *J* = 7.2 Hz, 6H), 0.68 (t, *J* = 6.9 Hz, 6H). $^{13}$C NMR (125 MHz, $CDCl_3$) δ 186.06, 159.83, 158.03, 155.20, 153.84, 153.21, 153.10, 146.45, 146.29, 138.42, 137.27, 136.49, 136.25, 135.38, 134.37, 133.46, 133.26, 131.94, 130.52, 129.27, 126.51, 121.66, 119.58, 114.96, 68.23, 55.99, 39.56, 31.97, 31.95, 31.78, 31.64, 31.50, 30.85, 30.32, 30.21, 30.10, 29.78, 29.68, 29.60, 29.56, 29.39, 29.34, 25.93, 22.70, 22.64, 14.14, 14.12. HRMS (m/z) $[M]^+$ calcd. For ($C_{112}H_{124}Cl_2F_4N_8O_3S_4$): 1902.7992. Found: 1902.7996.

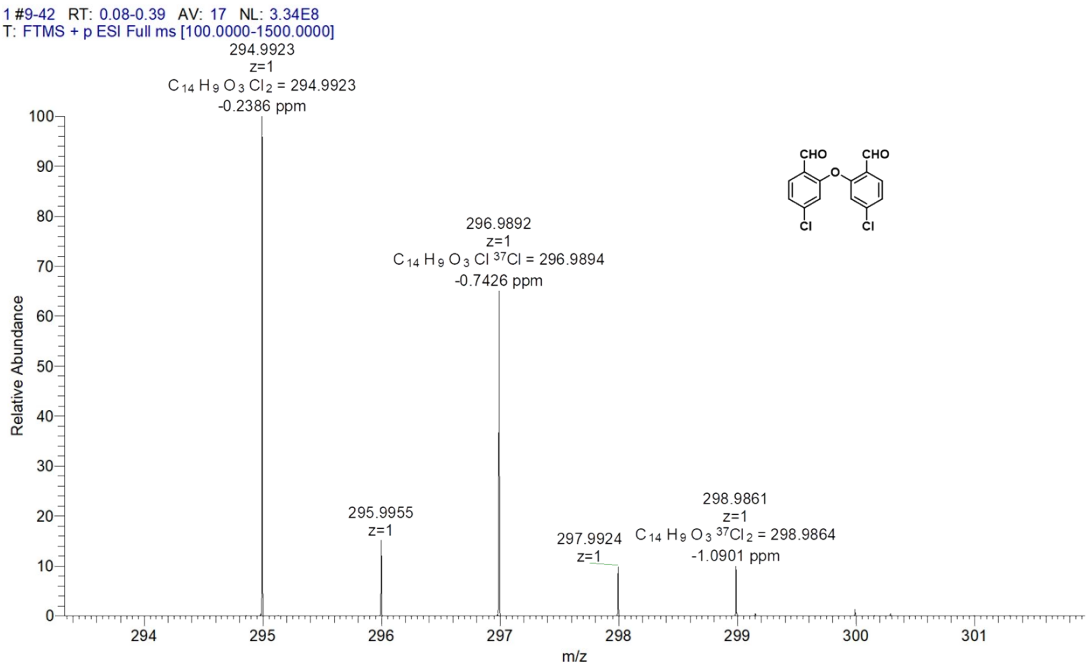


**Figure S1**. HRMS spectrum of compound ***m*-3.**

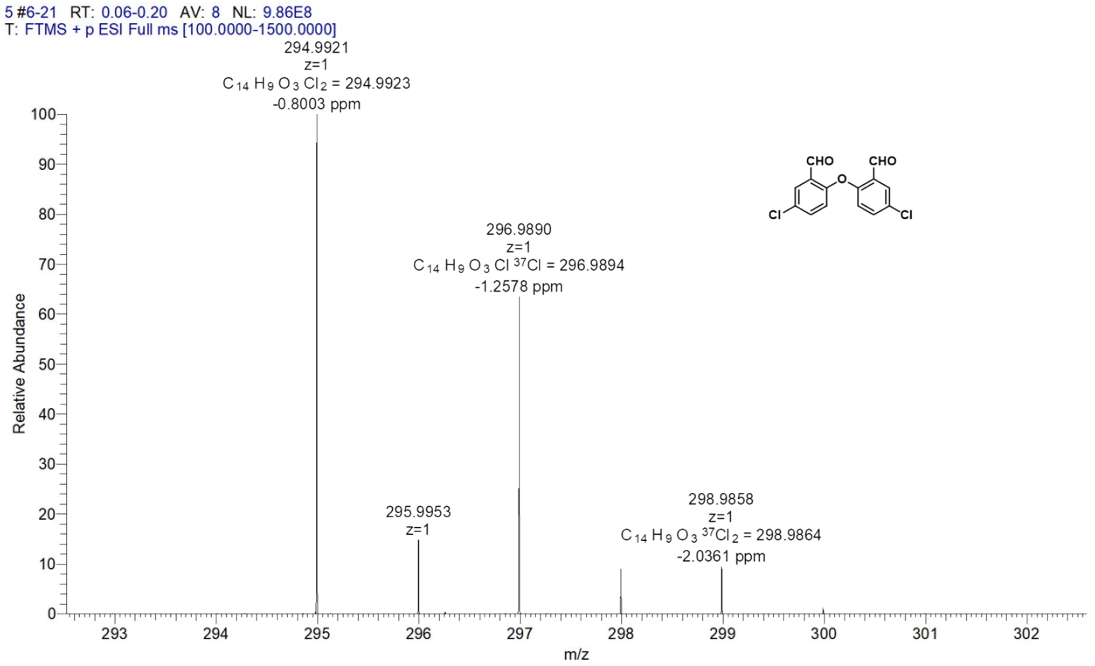


**Figure S2**. HRMS spectrum of compound ***p*-3.**

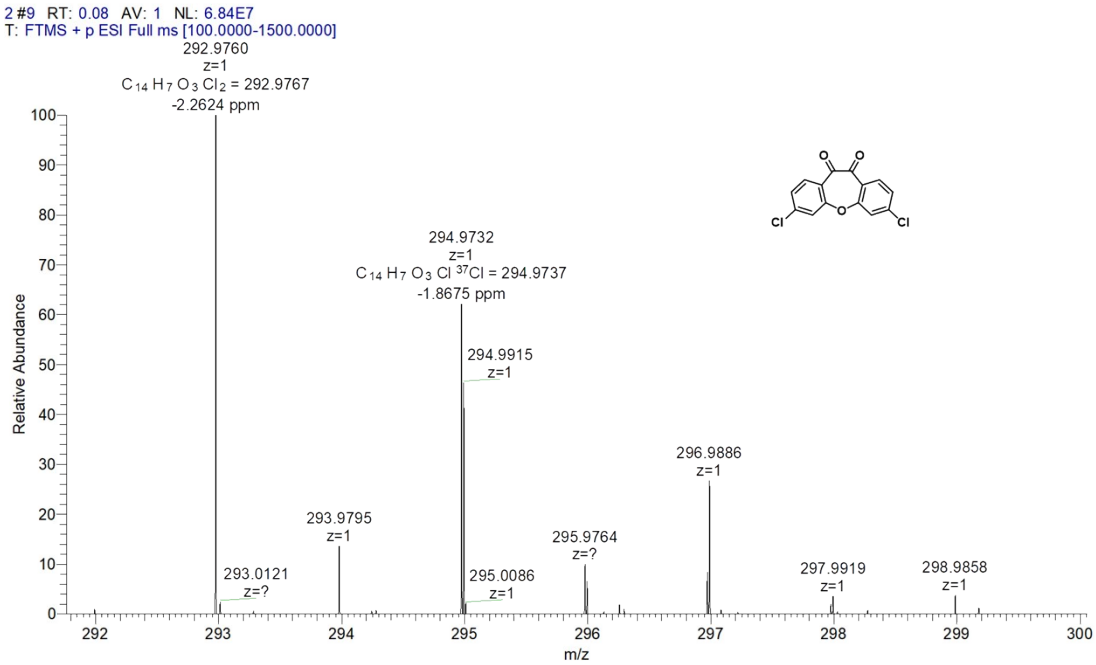


**Figure S3**. HRMS spectrum of compound ***m*-4.**

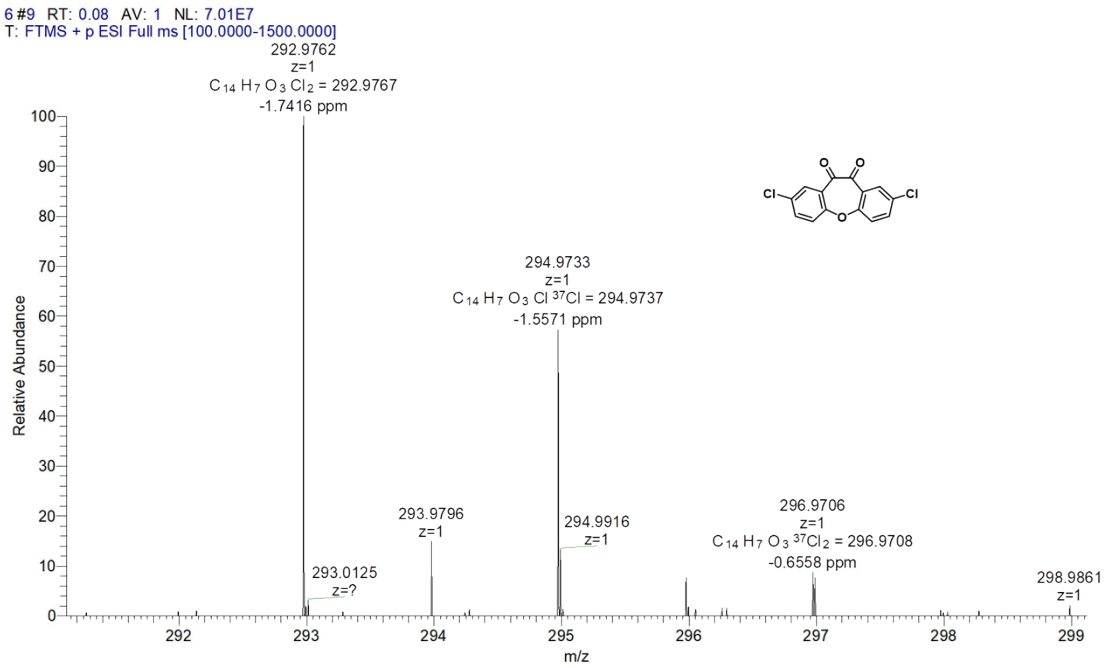


**Figure S4**. HRMS spectrum of compound ***p*-4.**

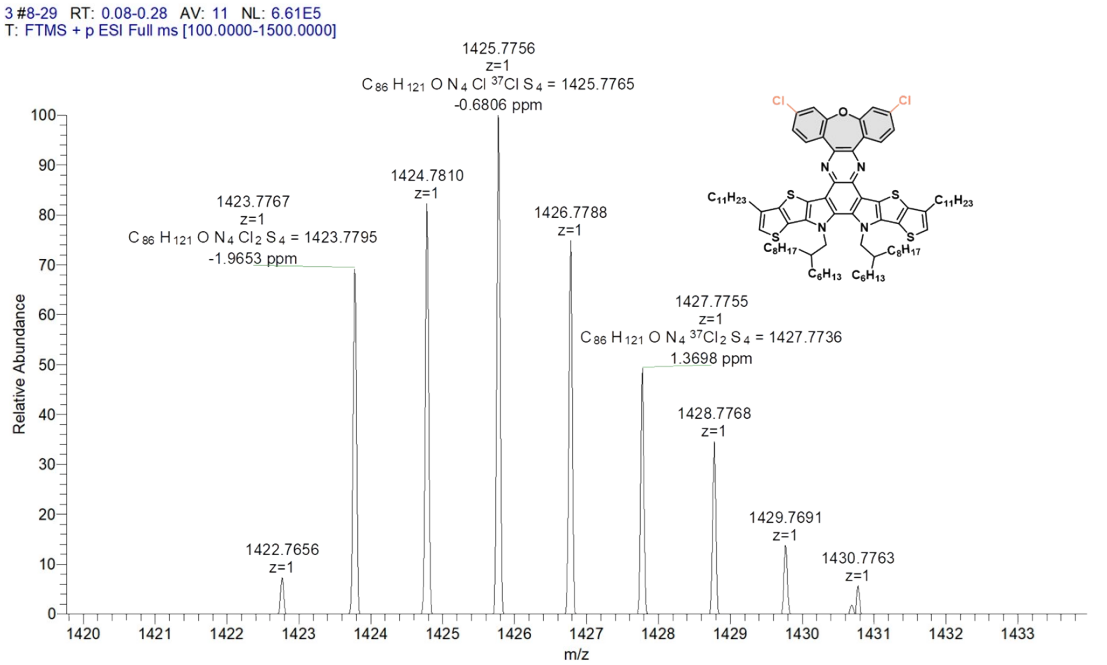


**Figure S5**. HRMS spectrum of compound ***m*-5.**

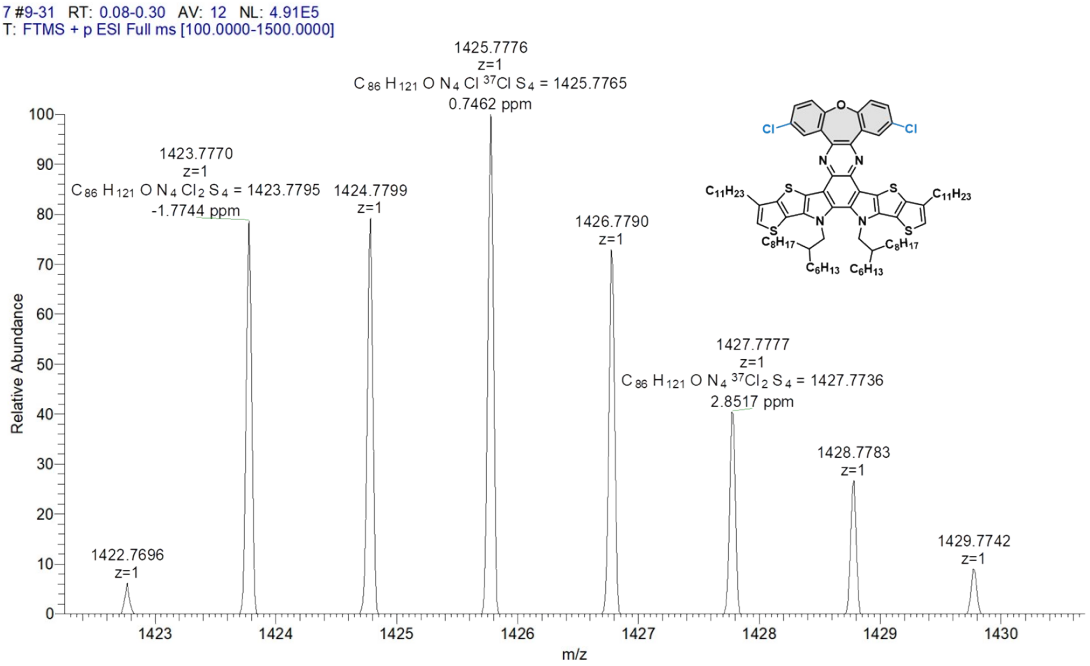


**Figure S6**. HRMS spectrum of compound ***p*-5.**

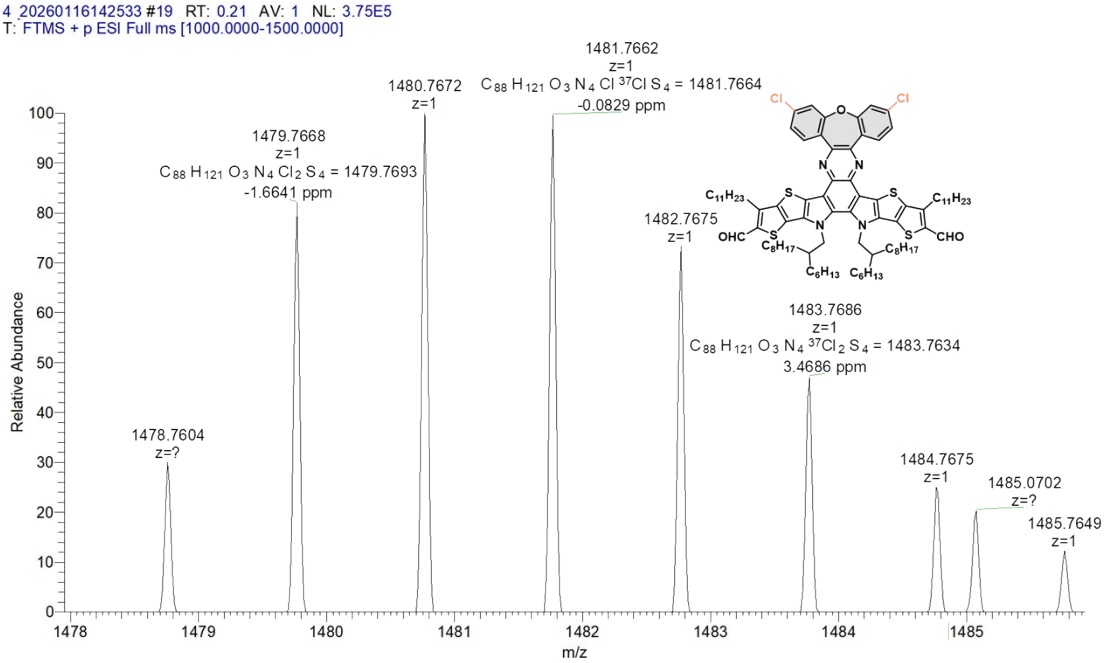


**Figure S7**. HRMS spectrum of compound ***m*-6.**

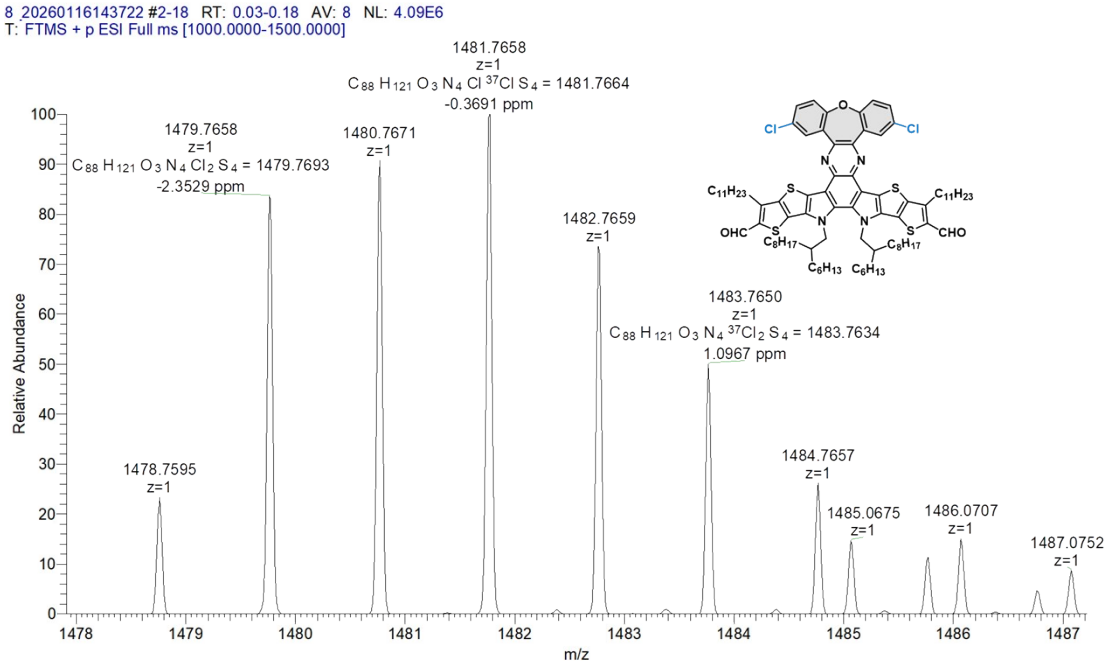


**Figure S8**. HRMS spectrum of compound ***p*-6.**

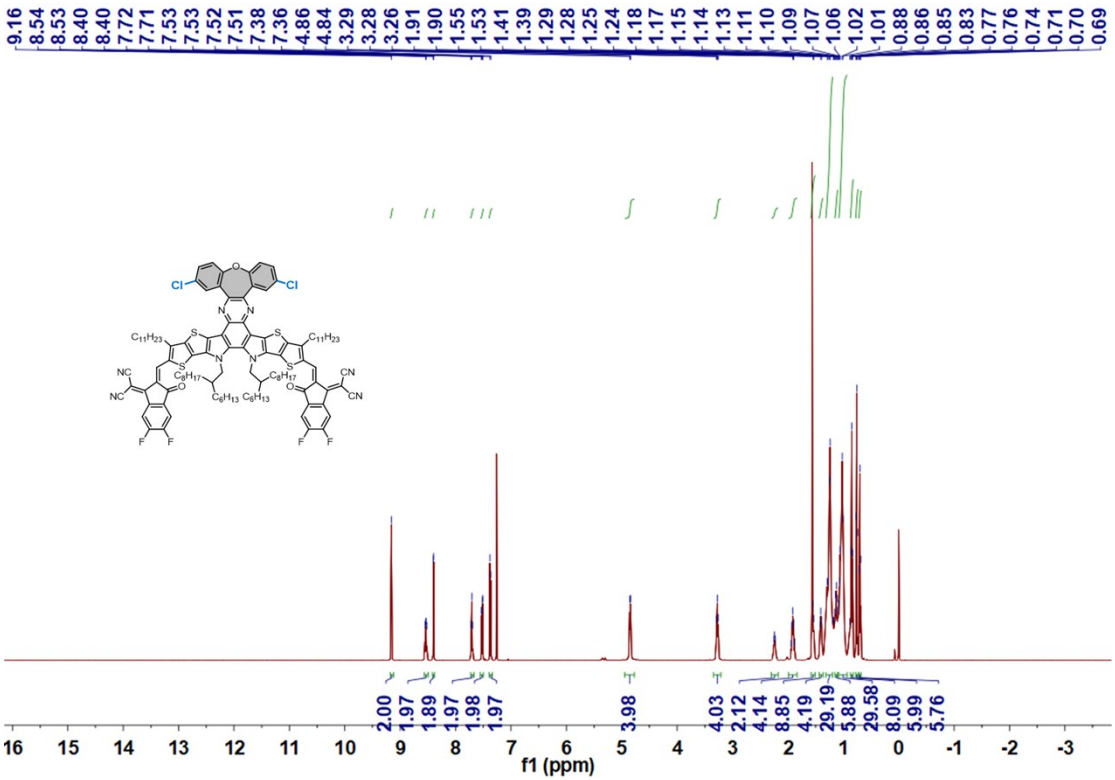


**Figure S9**. $^{1}$H NMR spectrum of compound ***p*-Cl-DOP** in $CDCl_3$.

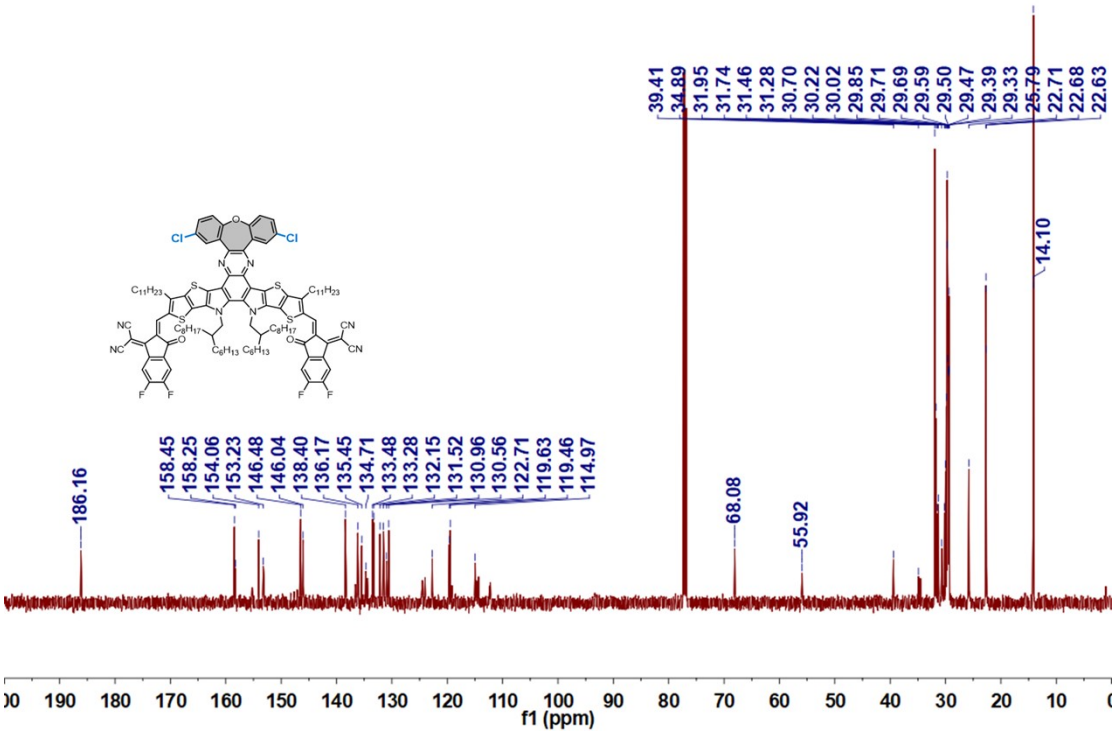


**Figure S10**. $^{13}C$ NMR spectrum of compound ***p*-Cl-DOP** in $CDCl_3$.

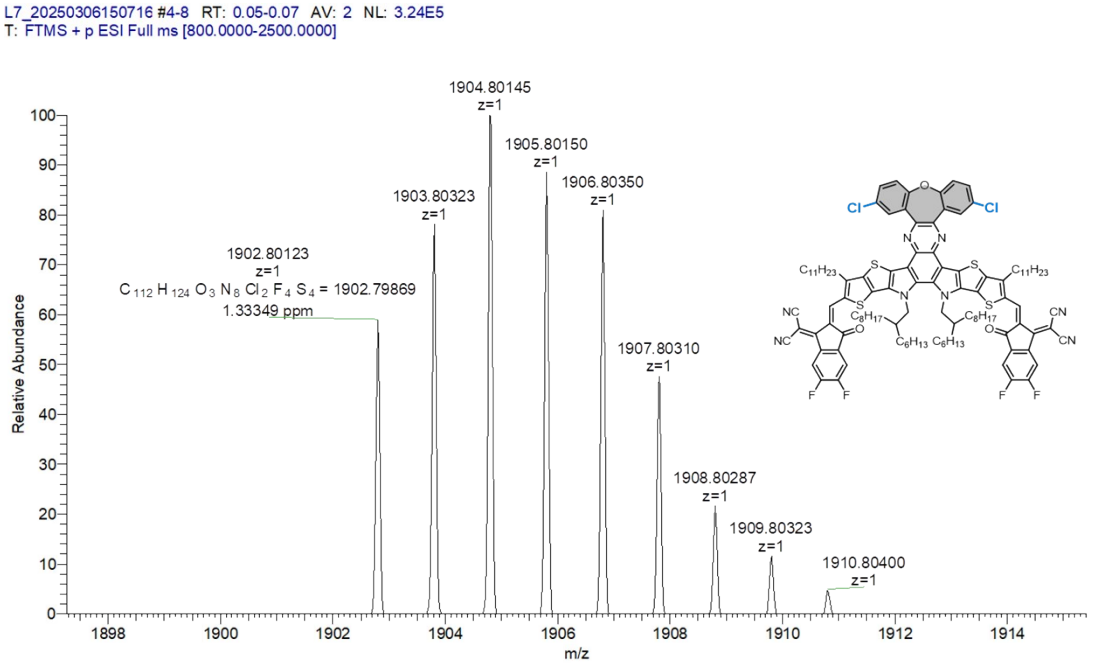


**Figure S11**. HRMS spectrum of compound ***p*-Cl-DOP**

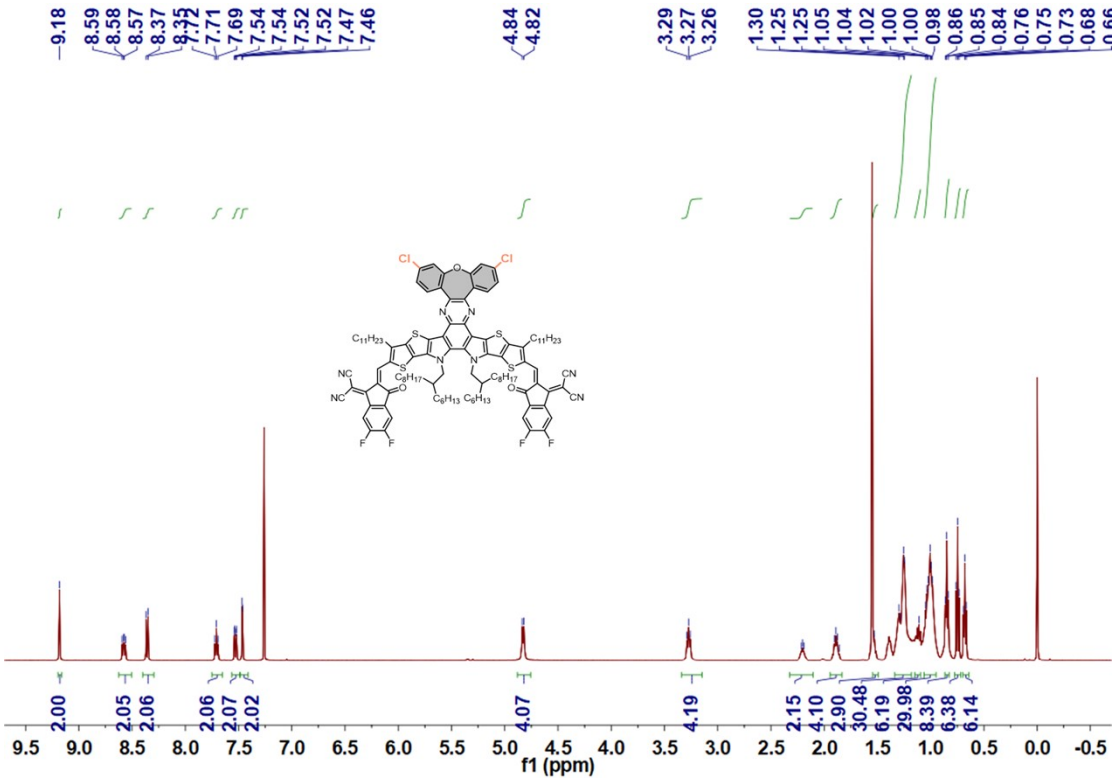


**Figure S12**. $^{1}$H NMR spectrum of compound ***m*-Cl-DOP** in $CDCl_3$.

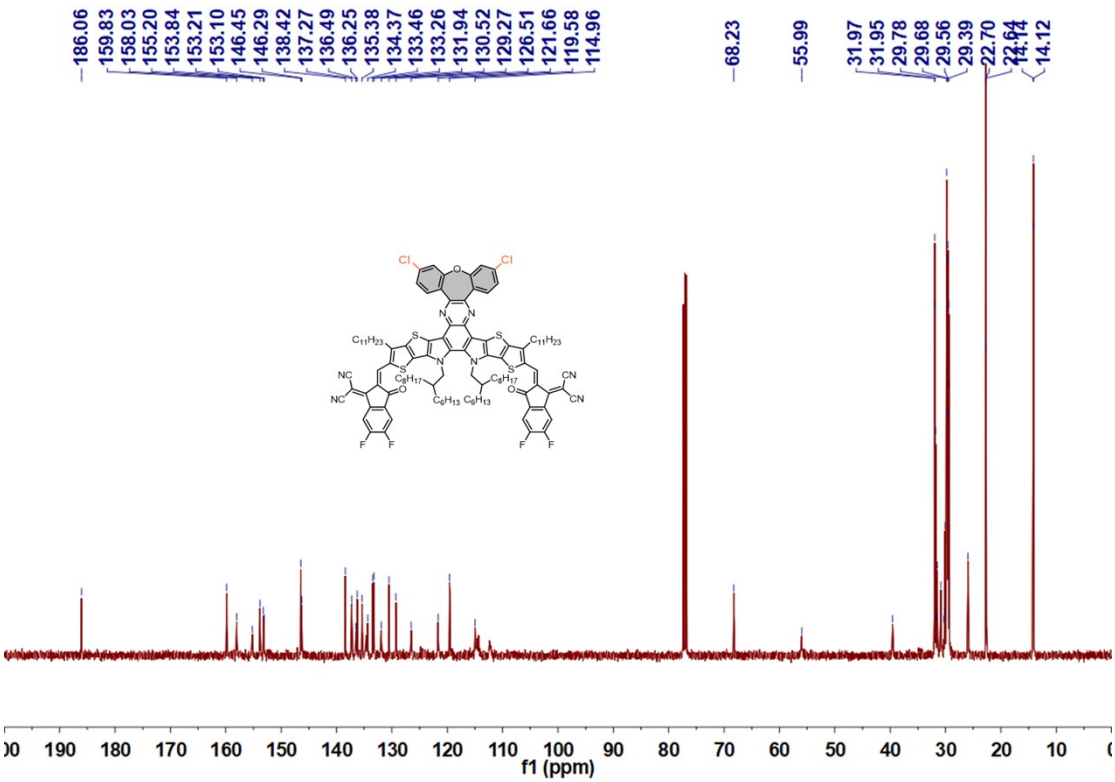


**Figure S13**. $^{13}$C NMR spectrum of compound ***m*-Cl-DOP** in $CDCl_3$.

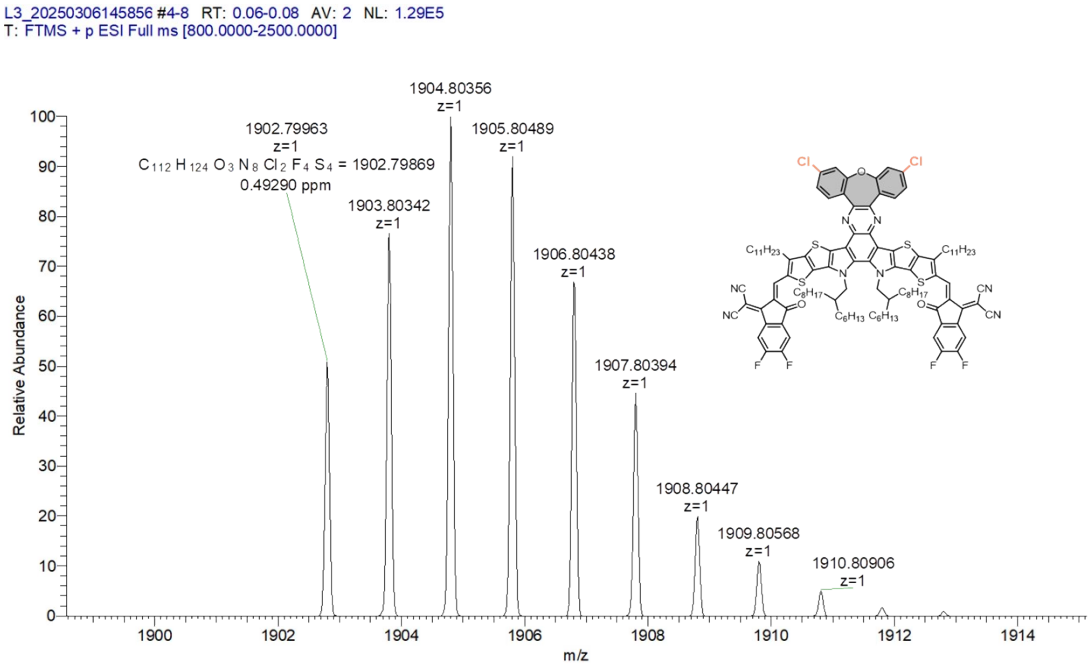


**Figure S14**. HRMS spectrum of compound ***m*-Cl-DOP**

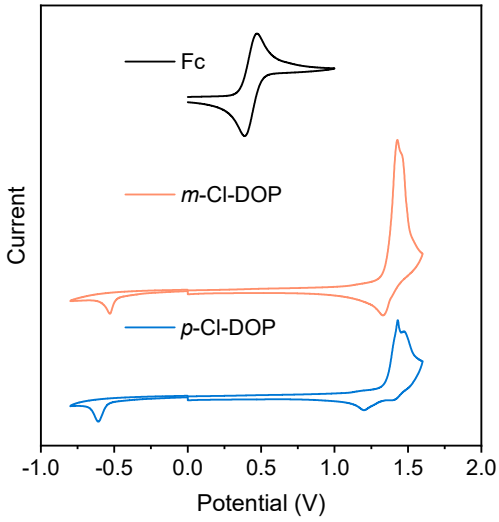


Figure S15. The CV curves of Fc, ***m*-Cl-DOP** and ***p*-Cl-DOP**.

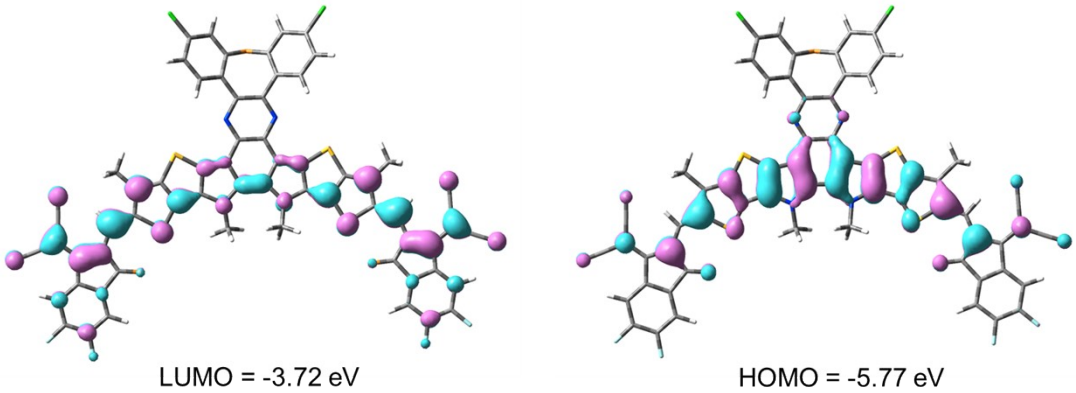

Figure S16. TD-DFT calculation result of ***m*-Cl-DOP**

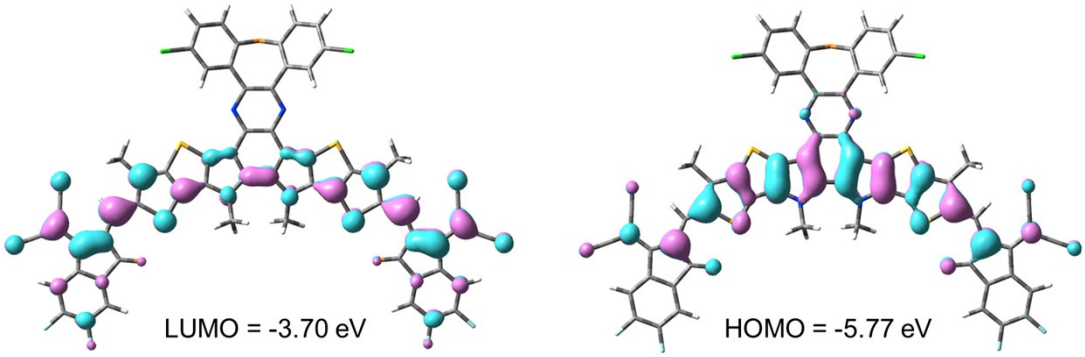


Figure S17. TD-DFT calculation result of ***p*-Cl-DOP**

**Table S1** The optical properties, LUMO/HOMO energy level of ***p*-Cl-DOP** and ***m*-Cl-DOP**

| Acceptor | $\lambda_{max}$ (nm)[a] | $\lambda_{max}$ (nm)[b] | $E_g$ (eV) | $E_{HOMO}$ (eV) | $E_{LUMO}$ (eV) |
|---|---|---|---|---|---|
| *p*-Cl-DOP | 732 | 795 | 1.90 | -5.72 | -3.82 |
| *m*-Cl-DOP | 735 | 804 | 1.84 | -5.72 | -3.88 |

a: Measured in chloroform solution at 25 °C ($1\times10^{-5}$ M) , b: measured in the thin film

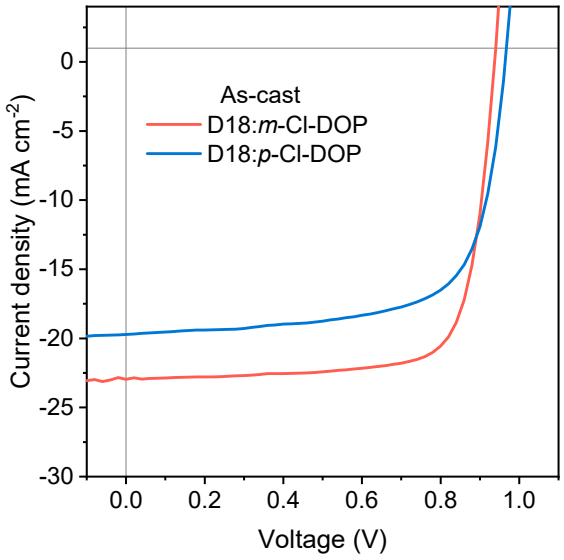


Figrue S18. current-voltage (J-V) characteristics under as-cast.

Table S2. Photovoltaic parameters of D18: m-Cl-DOP and D18: p-Cl-DOP based OSCs under as-cast.

| Active layer | $V_{OC}$ (V) | $J_{SC}$ (mA cm$^{-2}$) | FF (%) | PCE (%) |
|---|---|---|---|---|
| D18: *m*-Cl- | 0.934 | 23.23 | 77.31 | 16.78 |

| | | | | |
|---|---|---|---|---|
| DOP | | | | |
| D18: *p*-Cl-DOP | 0.964 | 19.73 | 69.59 | 13.23 |

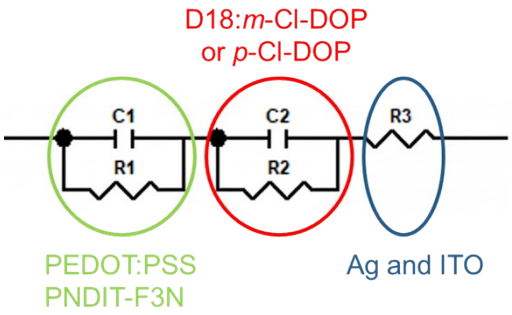


Figure S19. The equivalent circuit for fitting impedance spectroscopy.

Table S3. Fitting parameters of impedance spectroscopy using equivalent circuit.

| | $R_s$ [Ω] | $C_1$ [nF] | $R_1$ [Ω] | $C_2$ [nF] | $R_2$ [Ω] |
|---|---|---|---|---|---|
| D18:*p*-Cl-DOP | 27.69 | 4.0 | 823 | 6.1 | 135 |
| D18:*m*-Cl-DOP | 21.13 | 5.4 | 431 | 5.4 | 54 |

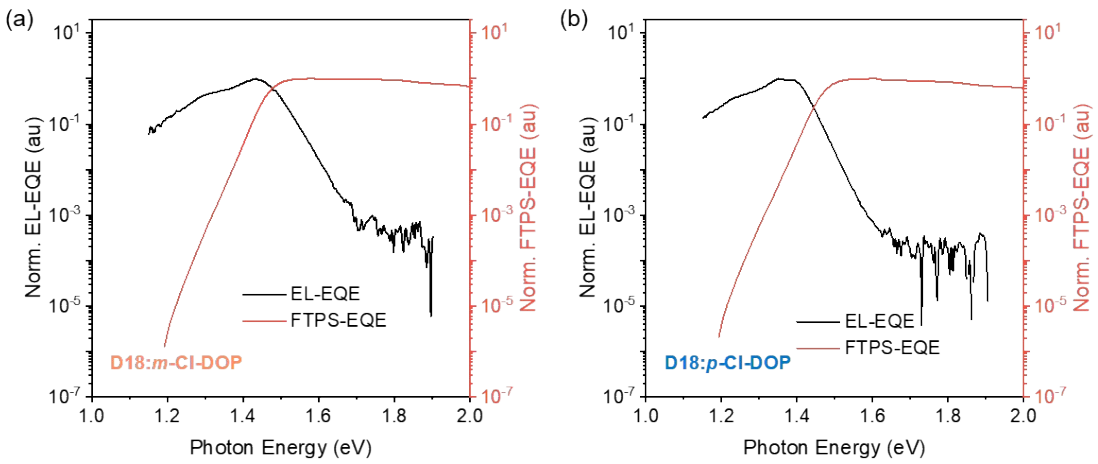


Figure S20. Semi-logarithmic plots of normalized EL and measured EQE by FTPS as a function of energy for (a) ***m*-Cl-DOP** and (b) ***p*-Cl-DOP** devices.

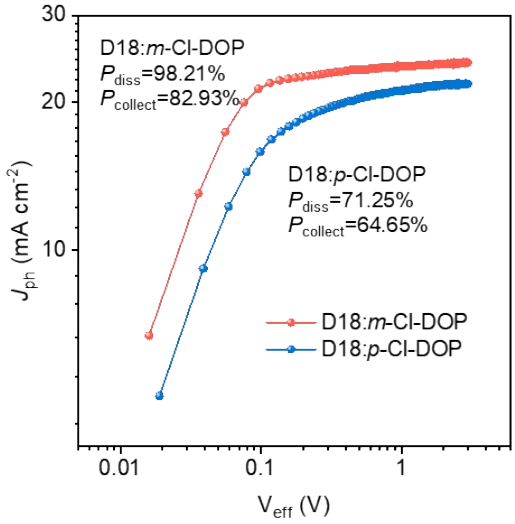


**Figure S21.** The $J_{ph}$ - $V_{eff}$ curves.

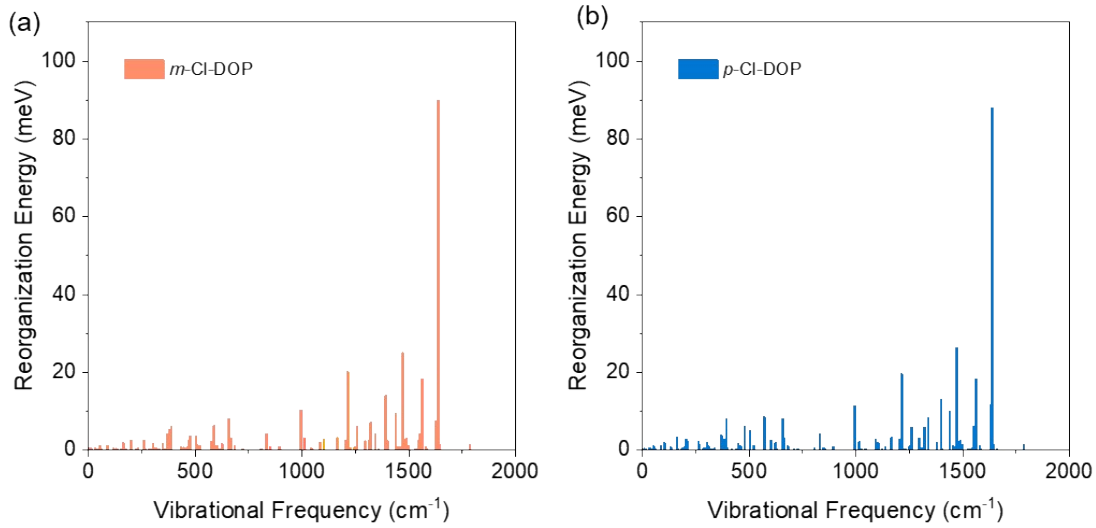


Figure S22. Calculated reorganization energies versus the vibrational frequency of (a) ***m*-Cl-DOP** and (b) ***p*-Cl-DOP**.

Table S4. Detailed $E_{loss}$ parameters in **D18:*m*-Cl-DOP** and **D18:*p*-Cl-DOP** devices

| | $V_{OC}$[a)] (V) | $E_g$[b)] (eV) | $qV_{loss}$ (eV) | $V_{OC}^{SQ}$[c)] (V) | $V_{OC}^{rad}$[d)] (V) | $\Delta E_1$ (eV) | $\Delta E_2$[e)] (eV) | $\Delta E_3$[f)] (eV) |
|---|---|---|---|---|---|---|---|---|
| D18:*p*-Cl-DOP | 0.961 | 1.470 | 0.509 | 1.205 | 1.155 | 0.265 | 0.049 | 0.195 |
| D18:*m*-Cl-DOP | 0.936 | 1.468 | 0.540 | 1.203 | 1.159 | 0.265 | 0.044 | 0.231 |

a) $V_{OC}$: measured in the voltage loss test without an aperture.

b) $E_g$: optical bandgaps, via the derivatives of the EQE spectra (dEQE/dE).

c) $Voc^{SQ}$: Schokley-Queisser limit to $V_{OC}$.

d) $Voc^{rad}$: radiative limit to $V$oc, measured using $EQE_{EL}$

e) $\Delta E_2$ ($(Voc^{SQ}$-$Voc^{rad})$: voltage losses due to non-ideal absorption (it was calculated from EL and FTPS

measurements).

f) $\Delta E_3$ ($\Delta Voc^{non-rad}$): voltage losses due to non-radiative recombination only.

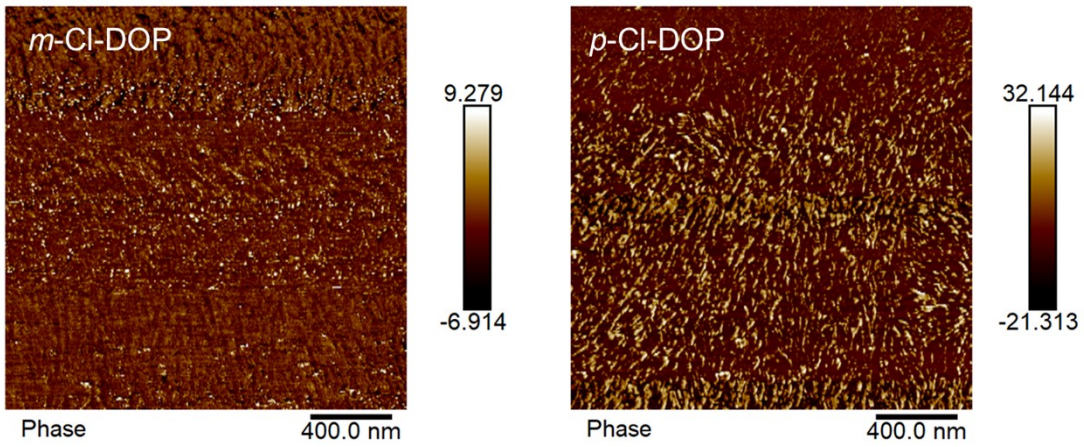


Figure S23. AFM phase image for the D18:*m*-Cl-DOP and D18:*p*-Cl-DOP blend films.

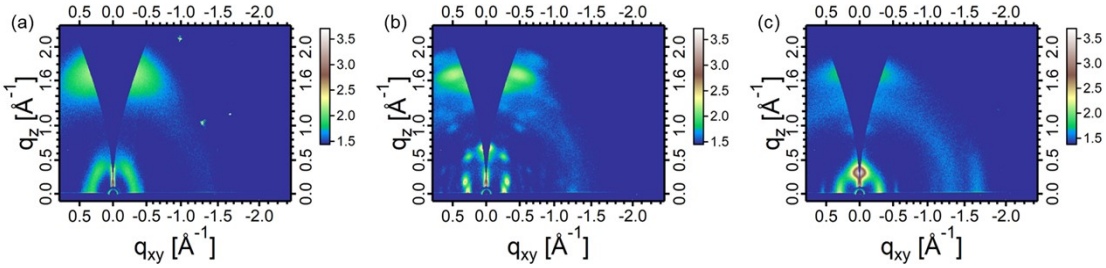


Figure S24. 2D GIWAXS patterns of (a) ***m*-Cl-DOP**; (b) ***p*-Cl-DOP** and (c) **D18** films.

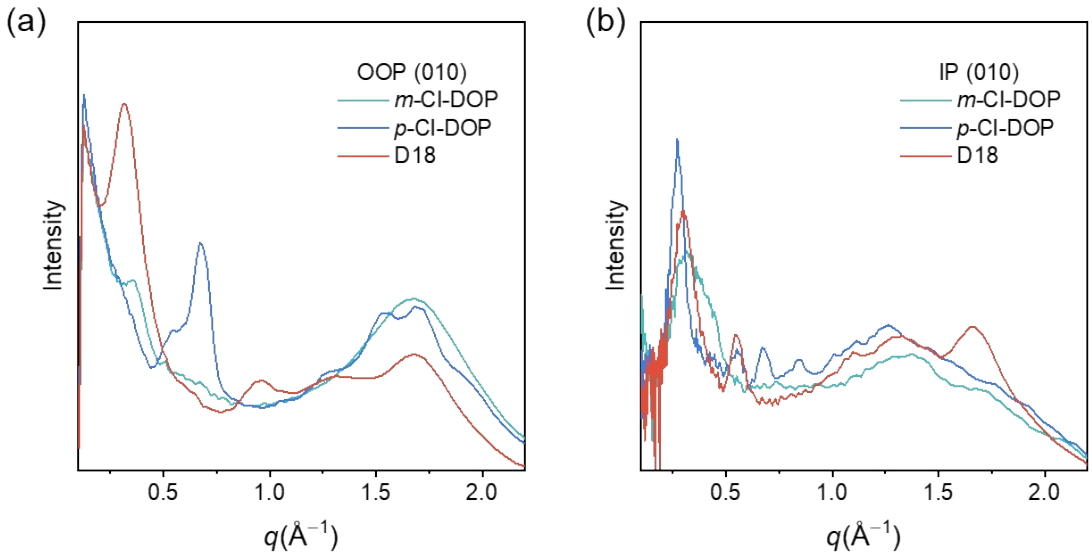


Figure S25. 1D GIWAXS line-cuts of pure ***m*-Cl-DOP, *p*-Cl-DOP** and **D18** film.

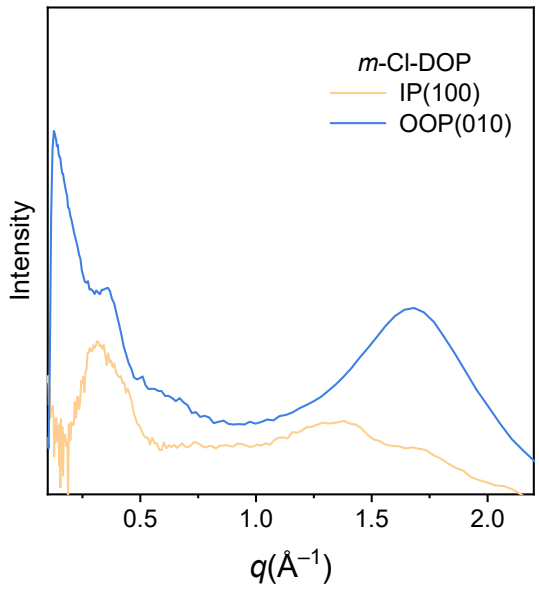


Figure S26. 1D GIWAXS line-cuts of pure ***m*-Cl-DOP** film.

Table S5. The detailed data of OOP (010) diffraction peaks of **D18:*m*-Cl-DOP** and **D18:*p*-Cl-DOP** blend films and ***m*-Cl-DOP** film.

| | *q* (Å$^{-1}$) | *d* (Å) | FWHM (Å$^{-1}$) | CCL (Å) |
|---|---|---|---|---|
| ***m*-Cl-DOP** | 1.682 | 3.74 | 0.323 | 17.51 |
| **D18:*m*-Cl-DOP** | 1.628 | 3.86 | 0.224 | 25.24 |
| **D18:*p*-Cl-DOP** | 1.655 | 3.80 | 0.289 | 19.57 |

Table S6. The detailed data of IP (100) diffraction peaks of **D18:*m*-Cl-DOP** and **D18:*p*-Cl-DOP** blend films.

| | *q* (Å$^{-1}$) | *d* (Å) | FWHM (Å$^{-1}$) | CCL (Å) |
|---|---|---|---|---|
| ***m*-Cl-DOP** | 0.105 | 59.84 | 0.033 | 171.36 |
| **D18:*m*-Cl-DOP** | 0.134 | 46.89 | 0.039 | 145.00 |
| **D18:*p*-Cl-DOP** | 0.133 | 47.24 | 0.042 | 134.64 |

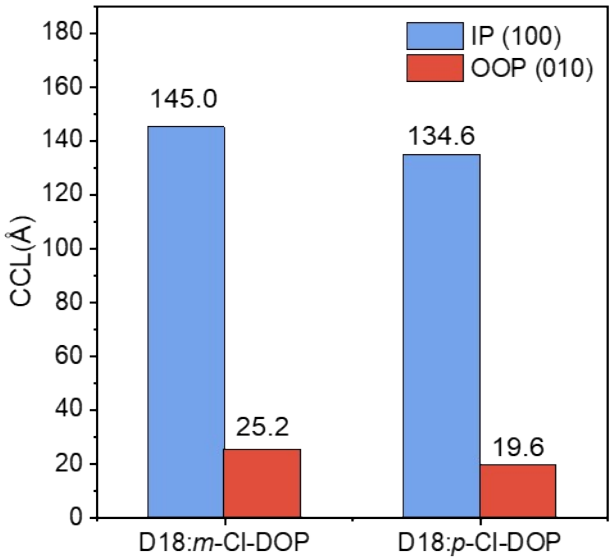


Figure S27. CCL histograms for (100) peak (in-plane) and (010) peak (out-of-plane) of **D18:*m*-Cl-DOP** and **D18:*p*-Cl-DOP** blend films.

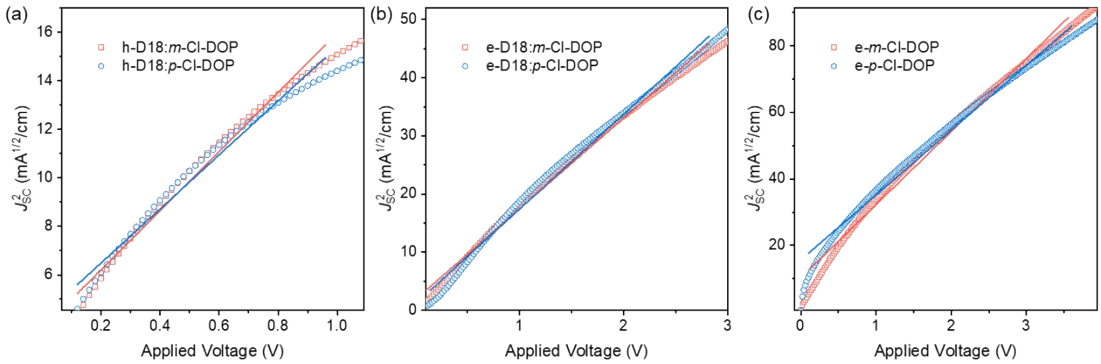


**Figure S28.** J-V curve of a) hole devices; (b) electronics devices; (c) pure acceptor thin-film electronic devices.

## reference

1. K. Satyam, J. Ramarao and S. Suresh, *Organic & Biomolecular Chemistry*, 2021, **19**, 1488-1492.
2. H. Tian, K. Sun, D. Luo, Y. Wang, Z. Chen, L. Yu, G. Zhang, C. Yang and Z. Luo, *Science China Chemistry*, 2025, **68**, 6628-6638.